Performance Analysis of Fifth-Generation Cellular Uplink

Don Torrieri,* Salvatore Talarico,† and Matthew C. Valenti†
*U.S. Army Research Laboratory, Adelphi, MD, USA
†West Virginia University, Morgantown, WV, USA

***Abstract*—Fifth-generation cellular networks are expected to exhibit at least three primary physical-layer differences relative to fourth-generation ones: millimeter-wave propagation, antenna-array directionality, and densification of base stations. In this paper, the effects of these differences on the performance of single-carrier frequency-domain multiple-access uplink systems with frequency hopping are assessed. A new analysis, which is much more detailed than any other in the existing literature and accommodates actual base-station topologies, captures the primary features of uplink communications. Distance-dependent power-law, shadowing, and fading models based on millimeter-wave measurements are introduced. The beneficial effects of base-station densification, highly directional sectorization, and frequency hopping are illustrated.**

I. Introduction

This paper provides a performance analysis of the uplink of a fifth-generation cellular network in its primary mode of operation. It is assumed that millimeter-wave frequencies will be adopted, but that the basic structure of the fourth-generation (4G) single-carrier frequency-domain multiple-access (SC-FDMA) uplink systems will be maintained. The first assumption is widely supported in the current literature on fifth-generation (5G) systems [1], [2]. The second one is based on the favorable characteristics of SC-FDMA and the critical importance of transmitter power efficiency, which is enabled by the low peak-to-average power ratio of SC-FDMA and similar single-channel modulations [3], [4]. It is further assumed that 5G systems will exploit frequency hopping, as is done in 4G/LTE systems [5].

The analysis in this paper applies the methodology of [6], which we call deterministic geometry. Unlike stochastic geometry, deterministic geometry can accommodate arbitrary topologies with distance-dependent propagation models. The distance dependence of the propagation and fading models accounts for the fact that mobiles close to the base station have a line-of-sight (LOS) path, but the more distant mobiles do not.

The *conditional* outage probability of a SC-FDMA uplink is derived, where the conditioning is with respect to an arbitrary network topology. In the numerical examples, we use an actual deployment of the base stations. Each simulation trial generates a network realization in which the mobile placements are drawn from the uniform clustering distribution with each mobile having an exclusion zone [6]. For each realization of the network, the outage probability is computed for a reference link. By averaging over many network realizations, the average outage probability and other statistical performance measures are computed.

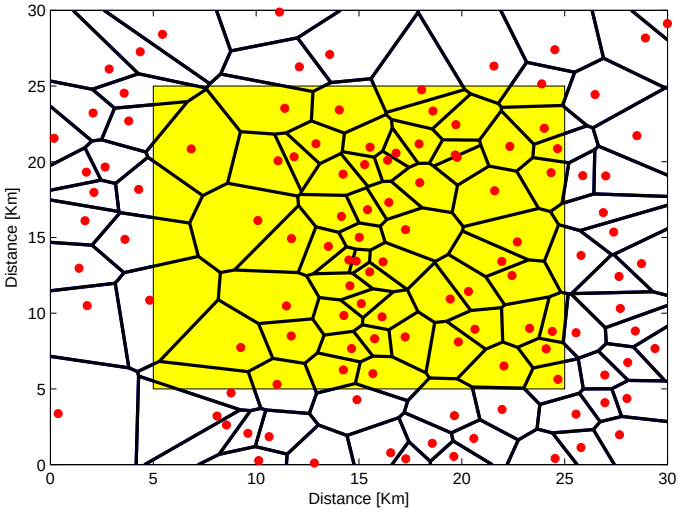

Fig. 1. Actual base station locations from a current cellular deployment. Base stations are represented by large circles, and Voronoi cell boundaries are represented by thick lines.

The remainder of the paper is organized as follows. Section II describes the system model, which accounts for distance dependent fading, path loss, and shadowing based on millimiter-wave measurements, and for highly directional antennas and sectorization. Section III provides a closed-form expression for the conditional outage probability. Section IV provides a numerical evaluation of a 5G system. Finally, the paper concludes in Section V.

II. Network Model

In the network model, C base stations and M mobiles are confined to a finite area. As an example, Fig. 1 depicts an actual deployment of $C = 121$ base stations extracted from a database of base-station locations in the United Kingdom. Base stations are represented by large circles, and Voronoi cell boundaries are represented by thick lines. The network occupies 900 km^2 inside a square.

For practical reasons such as the high propagation loss and the complexity of channel state estimation at millimeter-wave frequencies, the antenna arrays at the base stations and mobiles exploit beamforming rather than spatial multiplexing for uplink transmissions [7]. Densification, high mobility, and

the severe impact of blockages at millimeter-wave frequencies cause frequent handoffs and hence the need for rapid beam alignments. Sectorization, which is the division of base-station coverage into ζ fixed angular sector beams centered at the base station, is used to reduce beam-alignment delays and pilot contamination. At millimeter-wave frequencies, the beams can be implemented using many antenna elements, perhaps hundreds, and hence have narrow beamwidths and very small sidelobes and backlobes. Each mobile transmits through an adaptive and highly directional antenna array.

The scalar $S_l,\ l = 1, 2, ..., \zeta C$, represents the lth sector or its receiver, and the scalar $X_i,\ i = 1, 2, ..., M$, represents the ith mobile. The vector $\mathbf{S}_l,\ l = 1, 2, ..., \zeta C$, represents the location of the lth sector receiver, and the vector $\mathbf{X}_i$, $i = 1, 2, ..., M$, represents the location of the ith mobile. The *normalized sector beam pattern* associated with S_l is

$$B_l(\theta) = \begin{cases} 1, & \psi_l \le \theta \le \psi_l + 2\pi/\zeta \\ b, & otherwise \end{cases} \tag{1}$$

where ψ_l is the offset angle of the beam pattern, and b is the relative sidelobe and backlobe level.

Let $\mathcal{X}_l$ denote the set of mobiles served by sector S_l. Let $X_r \in \mathcal{X}_j$ denote a reference mobile that transmits a desired signal to a reference receiver S_j. Let $\mathrm{g}(i)$ denote a function that returns the index of the sector serving X_i so that $X_i \in \mathcal{X}_l$ if $\mathrm{g}(i) = l$. The sector $S_{\mathrm{g}(i)}$ that serves mobile X_i is assumed to be the one with minimum local-mean path loss when the mainlobe of the transmit beam of X_i is aligned with the sector beam of $S_{\mathrm{g}(i)}$. Thus, the serving sector has index

$$\mathrm{g}(i) = \arg\max_l \left\{ 10^{\xi_{i,l}/10} f\left(||\mathbf{S}_l - \mathbf{X}_i||\right),\ X_i \in \mathcal{A}_l \right\} \tag{2}$$

where $\xi_{i,l}$ is a *shadowing factor* for the link from X_i to S_l, $f(\cdot)$ is the area-mean path-loss function, $||\cdot||$ is the Euclidean norm, and $\mathcal{A}_l$ denote the set of mobiles *covered* by the sector beam of S_l. In the absence of shadowing, the serving sector will be the receiver that is closest to X_i. In the presence of shadowing, a mobile may actually be associated with a sector that is more distant than the closest one if the shadowing conditions are sufficiently better.

The area-mean path-loss function is a function of the distance d between a source and destination and is expressed as the attenuation power law

$$f(d) = \left(\frac{d}{d_0}\right)^{-\alpha(d)}, \quad d \ge d_0 \tag{3}$$

where $\alpha(d)$ is the attenuation power-law exponent, and d_0 is a reference distance that is less than or equal to the minimum of the near-field radius and the exclusion-zone radius of a mobile.

The distance-dependent model of the power-law exponent for millimeter-wave frequencies takes into account the area-mean attenuation due to blockages and reflections that occur over network links. This model reflects the empirical fact that $\alpha(d)$ differs substantially for LOS and non-line-of-sight (NLOS) links, tending toward $\alpha_{\min}$ for the usually shorter LOS links and tending toward a much larger $\alpha_{\max}$ for the usually longer NLOS links [8], [9], [10]. Empirical data indicates that usually there is a small range of link lengths for which there are both LOS and NLOS links. Therefore, $\alpha(d)$ is modeled as a monotonically increasing function:

$$\alpha(d) = \alpha_{\min} + (\alpha_{\max} - \alpha_{\min}) \tanh(\mu d) \tag{4}$$

which indicates that $\alpha_{\min} \le \alpha(d) < \alpha_{\max}$. The parameter μ controls the transition rate from $\alpha_{\min}$ to a value close to $\alpha_{\max}$.

Local-mean large-scale terrain effects are included in the shadowing model. The shadowing factor can be derived from a deterministic terrain model or can be modeled as a random variable in a statistical model. In this paper, we assume lognormal shadowing in which the $\{\xi_{i,j}\}$ are independent, identically distributed, zero-mean Gaussian random variables with a distance-dependent variance.

For millimeter-wave frequencies, empirical data [8], [9], [10] indicates that the effect of the shadowing increases for the usually longer NLOS links. Since there is a small range of link lengths for which there are both LOS and NLOS links, the standard deviation of the shadowing factor for millimeter-wave frequencies is modeled as a monotonically increasing function:

$$\sigma_s(d) = \sigma_{\min} + (\sigma_{\max} - \sigma_{\min}) \tanh(\mu d) \tag{5}$$

which indicates that $\sigma_{\min} \le \sigma_s(d) < \sigma_{\max}$.

The fading is assumed to have a Nakagami distribution function. Since the fading becomes more severe for the longer links, the distance-dependent Nakagami parameter is modeled as a monotonically decreasing function:

$$m(d) = m_{\max} - (m_{\max} - m_{\min}) \tanh(\mu d) \tag{6}$$

which indicates that $m_{\min} \le m(d) < m_{\max}$.

Frequency hopping [11] is used in SC-FDMA uplink systems to provide the diversity that will mitigate the effects of frequency-selective fading and intersector interference. Because of network synchronization and similar propagation delays for the mobiles associated with a cell sector, synchronous orthogonal frequency-hopping patterns can be allocated so that at any given instant in time, there is no *intrasector* interference. The frequency-hopping patterns transmitted by mobiles in other sectors are not generally orthogonal to the patterns in a reference sector, and hence produce *intersector* interference. The varying propagation delays from the interfering mobiles cause their frequency-hopping signals to be asynchronous with respect to the desired signal. Duplexing prevents uplink interference from downlink transmissions.

Each mobile uses a frequency-hopping pattern over a hopset with L disjoint frequency channels. Let $L_l,\ l = 1, 2, \ldots, \zeta C$, denote positive integer divisors of L such that $L/L_l \ge 2$. Each mobile in $\mathcal{X}_l$ is assigned a distinct block of L_l contiguous frequency channels during each of its hop intervals, and the block may change to any of L/L_l disjoint spectral regions with every hop. Consider an uplink *reference signal* that traverses a reference link from a reference mobile X_r to a reference

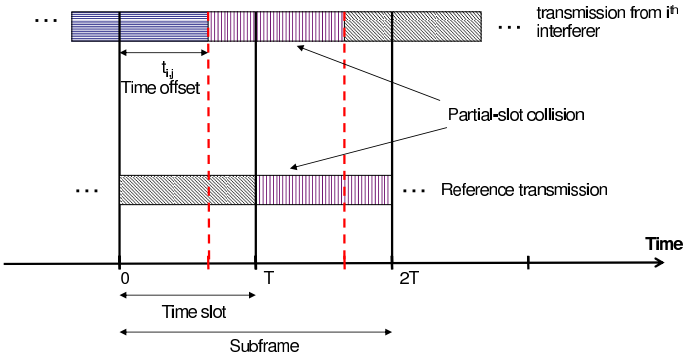

Fig. 2. Illustration of co-channel interference at base station S_j produced by an interfering mobile X_i arriving at the base station with a relative timing offset of $t_{i,j}$. Each block in the illustration represents a hop, and the selected channel is indicated by the shading of the block. A partial-slot collision is indicated, where the interfering mobile has selected the channels used by the reference mobile during the second slot of the subframe. However, due to the asynchronism, the collision only extends for part of the slot.

receiver S_j. Because of a possible incomplete spectral overlap, the received interference power from mobile X_i at S_j when the mobile's signal collides with the reference signal is reduced by the *spectral factor*

$$F_l = \min\left(L_j/L_l, 1\right). \tag{7}$$

Each active mobile points its antenna beam toward its base station. The beam pattern is modeled with two gains: one for the mainlobe and another for the sidelobes and backlobes. The *normalized beam gain* at the reference receiver S_j due to the angular offset of this beam pattern, is defined as

$$b_{i,j} = \begin{cases} 1, & \frac{(\mathbf{S}_j - \mathbf{X}_i)^T (\mathbf{S}_{\mathrm{g}(i)} - \mathbf{X}_i)}{||\mathbf{S}_j - \mathbf{X}_i|| ||\mathbf{S}_{\mathrm{g}(i)} - \mathbf{X}_i||} > \cos\left(\frac{\Theta}{2}\right) \\ a, & otherwise \end{cases} \tag{8}$$

where Θ is the beamwidth of the antenna mainlobe, superscript T denotes the transpose, and a is the sidelobe and backlobe level.

Associated with each potentially interfering mobile is a hop transition time $t_{i,j}$ at S_j relative to the hop transition time of a pair of hop intervals of the reference signal. Fig. 2 illustrates the relative timing between the reference mobile and the i^{th} interfering mobile. The reference mobile transmits a turbo codeword of duration $2T$, which is aligned with the subframe. It is assumed that the frequency separation of the two frequency channels of the two slots is sufficient for independent fading of fixed amplitude in each slot. If the base stations and mobiles are synchronized, then

$$t_{i,j} = [(||\mathbf{S}_j - \mathbf{X}_r|| - ||\mathbf{S}_j - \mathbf{X}_i||)/c] \bmod T \tag{9}$$

where c is the speed of an electromagnetic wave. As illustrated in Fig. 2, the reference signal encounters four time periods of potential interference from an active mobile X_i: $0 \le t \le t_{i,j}$, $t_{i,j} \le t \le T$, $T \le t \le t_{i,j} + T$, and $t_{i,j} + T \le t \le 2T$. The generic index $k \in \{1, 2, 3, 4\}$, denotes a time period of the subframe with duration that varies with each $t_{i,j}$. In the example provided in Fig. 2, co-channel interference occurs during the third time period, where the interfering mobile has selected the channels used by the reference mobile. The *fractional duration* of the each of the four subframe time periods relative to the subframe period $2T$ are

$$C_{i,j,k} = \begin{cases} \frac{t_{i,j}}{2T}, & k = 1, 3 \\ \frac{T - t_{i,j}}{2T}, & k = 2, 4 \end{cases}. \tag{10}$$

The set of indices of potentially interfering mobiles is $\mathcal{S} = \{i : X_i \notin \mathcal{X}_j\}$. Let N_l denote the number of mobiles associated with sector S_l. Because of the required orthogonality of frequency blocks assigned to mobiles within each sector, $N_l \le L/L_l$ and any additional mobiles within the sector are reassigned to other sectors. In view of the potential spectral overlaps, the maximum number of interfering mobiles within a sector during a subframe time period is $\min[\max\left(L_j/L_l, 1\right), N_l]$. Let $\mathcal{S}_k \subset \mathcal{S}$ denote the set of interfering mobiles during subframe time period k. If $N_l \le \max\left(L_j/L_l, 1\right)$, then all N_l mobiles in sector l are in $\mathcal{S}_k$. If $N_l > \max\left(L_j/L_l, 1\right)$, then some of the mobiles in sector l cannot cause interference during subframe time period k. In that case, we approximate by randomly selecting a subset of the N_l mobiles to be included in $\mathcal{S}_k$.

Let $q_{i,k}$ denote the probability that the signal from a potentially interfering mobile collides with the reference signal during subframe time period k, $1 \le k \le 4$. The *activity probability* p_i is the probability that mobile X_i is transmitting during time interval $[0, 2T)$. Assuming uniformly distributed frequency-hopping patterns that are orthogonal within each sector,

$$q_{i,k} = \frac{\max\left(N_{\mathrm{g}(i)} L_{\mathrm{g}(i)}, L_j\right)}{L} p_i, \quad i \in \mathcal{S}_k, \quad 1 \le k \le 4 \tag{11}$$

and $q_{i,k} = 0$, otherwise.

The instantaneous signal-to-interference-and-noise ratio (SINR) at sector receiver S_j when the desired signal is from $X_r \in \mathcal{X}_j$ fluctuates because potentially interfering signals do not always coincide with the reference signal in time or frequency. Pilot sequences are used to estimate the complex fading amplitudes in the receiver. Therefore, the performance of the reference receiver is primarily a function of the *average SINR* defined as the ratio of the average power of the signal to the average power of the noise and interference, where the average is over the time interval of a subframe and turbo codeword. Thus, the average SINR during a subframe is

$$\gamma_{r,j} = \frac{\overline{\rho}_{r,j}}{\mathcal{N} + \sum_{k=1}^{4} \sum_{i \in \mathcal{S}_k} I_{i,k} \rho_{i,j,k} C_{i,j,k}} \tag{12}$$

where $\mathcal{N}$ is the noise power, $\overline{\rho}_{r,j}$ is the average received power from reference mobile X_r, and $\rho_{i,j,k}$ is the received power from an interference signal that collides with the reference signal during subframe time period k. The indicators $I_{i,k}$ are Bernoulli random variables with probabilities

$$P[I_{i,k} = 1] = q_{i,k}, \; P[I_{i,k} = 0] = 1 - q_{i,k} \quad i \in \mathcal{S}_k, \quad 1 \le k \le 4. \tag{13}$$

Let $g_{i,j,k}$ denote the fading gain of the signal from mobile X_i at S_j during time interval k. Assuming that the bandwidths of the L/L_l and L/L_j disjoint spectral regions exceed the coherence bandwidth, the $\{g_{i,j,k}\}$ are independent for each hop with unit-mean, and $g_{i,j,k} = a_{i,j,k}^2$, where $a_{i,j,k}$ has a Nakagami distribution with distance-dependent parameter $m_{i,j}$. Let P_i denote the maximum power from X_i that could be received at the reference distance d_0 in the absence of fading and shadowing. Allowing for the spectral and beam factors, the received power from X_i at S_j, $i \in \mathcal{S}_k$, during time interval k is

$$\rho_{i,j,k} = P_i g_{i,j,k} 10^{\xi_{i,j}/10} f\left(||\mathbf{S}_j - \mathbf{X}_i||\right) b_{i,j} F_{\mathbf{g}(i)} B_j\left(\theta_{i,j}\right) \quad i \in \mathcal{S}_k, \quad 1 \le k \le 4 \tag{14}$$

where $\theta_{i,j}$ is the arrival angle at S_j of a signal from X_i, and $B_j\left(\theta_{i,j}\right)$ is the gain of the uplink beam pattern of S_j.

Let $g_{r,j,1}$ and $g_{r,j,2}$ denote the unit-mean power gains due to the independent fading of the frequency-hopping reference signal in subframe slots 1 and 2, respectively. The power gain of independent Nakagami fading with parameter $m_0 = m_{r,j}$ in each slot has the gamma density function:

$$f_{r,j}(x) = \frac{m_0^{m_0} x^{m_0-1} \exp\left(-m_0 x\right)}{\Gamma\left(m_0\right)} u\left(x\right) \tag{15}$$

where $u\left(x\right) = 1$, $x \ge 0$, and $u\left(x\right) = 0$, otherwise. The average power gain due to fading is $\overline{g}_{r,j} = \left(g_{r,j,1} + g_{r,j,2}\right)/2$. Using (15), we obtain the density function of $\overline{g}_{r,j}$:

$$f_0(x) = \frac{\left(2m_0\right)^{2m_0} x^{2m_0-1} \exp\left(-2m_0 x\right)}{\Gamma\left(2m_0\right)} u\left(x\right) \tag{16}$$

which is the power of a Nakagami random variable with parameter $2m_0$. This doubling of the Nakagami parameter indicates the beneficial effect of the frequency hopping in mitigating frequency-selective fading. The average received power from reference mobile X_r is

$$\overline{\rho}_{r,j} = P_r \overline{g}_{r,j} 10^{\xi_{r,j}/10} f\left(d_r\right) \tag{17}$$

where $d_r = ||\mathbf{S}_j - \mathbf{X}_r||$ is the length of the reference link.

Power control ensures that the local-mean power received from each mobile in a sector is equal to a constant. If this constant is the same for all sectors, then

$$P_r 10^{\xi_{r,j}/10} f\left(d_r\right) = P_i 10^{\xi_{i,\mathbf{g}(i)}/10} f\left(||\mathbf{S}_{\mathbf{g}(i)} - \mathbf{X}_i||\right), \quad i \in \mathcal{S}_k. \tag{18}$$

Substituting (14), (17), and (18) into (12), we obtain

$$\gamma_{r,j} = \frac{\overline{g}_{r,j}}{\Gamma_0^{-1} + \sum_{k=1}^{4} \sum_{i \in \mathcal{S}_k} I_{i,k} \Omega_{i,j} g_{i,j,k} C_{i,j,k}} \tag{19}$$

where

$$\Omega_{i,j} = b_{i,j} F_{\mathbf{g}(i)} B_j\left(\theta_{i,j}\right) \frac{10^{[\xi_{i,j} - \xi_{i,\mathbf{g}(i)}]/10} f\left(||\mathbf{S}_j - \mathbf{X}_i||\right)}{f\left(||\mathbf{S}_{\mathbf{g}(i)} - \mathbf{X}_i||\right)} \tag{20}$$

is the ratio of the interference power from X_i to the reference-signal power, and

$$\Gamma_0 = \frac{P_r}{\mathcal{N}} 10^{\xi_{r,j}/10} f\left(d_r\right) \tag{21}$$

is the signal-to-noise ratio (SNR) at the sector receiver when the fading is absent.

III. Outage Probability

Let β denote the minimum average SINR required for reliable reception of a signal from X_r at its serving sector receiver S_j, $j = \mathbf{g}(r)$. An *outage* occurs when the average SINR of a signal from X_r falls below β. The value of β sets a limit on the code-rate R of the uplink, which is expressed in units of bits per channel use (bpcu), and depends on the modulation and coding schemes, and the overhead losses due to pilots, cyclic prefixes, and equalization methods. The exact dependence of R on β can be determined empirically through tests or simulation.

The set of $\{\Omega_{i,j}\}$, $i \in \mathcal{S}_k$, for reference receiver S_j is represented by the vector $\mathbf{\Omega}_j$. Conditioning on $\mathbf{\Omega}_j$, the *outage probability* of a desired signal from $X_r \in \mathcal{X}_j$ that arrives at S_j is

$$\epsilon = P\left[\gamma_{r,j} \le \beta \middle| \mathbf{\Omega}_j\right]. \tag{22}$$

Because it is conditioned on $\mathbf{\Omega}_j$, the outage probability depends on the particular network realization, which has dynamics over timescales that are much slower than the fading or frequency hopping. We define

$$\beta_0 = 2\beta m_0, \quad z = \Gamma_0^{-1} \tag{23}$$

where the Nakagami parameter $m_0 = \lfloor m_{r,j} \rfloor$ for the reference uplink signal is assumed to be a positive integer. A derivation similar to the one in [6] yields

$$\epsilon = 1 - e^{-\beta_0 z} \sum_{s=0}^{2m_0-1} \left(\beta_0 z\right)^s \sum_{t=0}^{s} \frac{z^{-t}}{(s-t)!} H_t(\mathbf{\Omega}) \tag{24}$$

where

$$H_t(\mathbf{\Omega}) = \sum_{\substack{\ell_{ik} \ge 0 \\ \sum_{k=1}^{4} \sum_{i \in \mathcal{S}_k} \ell_{ik} = t}} \prod_{k=1}^{4} \prod_{i \in \mathcal{S}_k} G_{\ell_{ik}}(i,j,k) \tag{25}$$

the summations in (25) are over all sets of nonnegative indices that sum to t,

$$G_\ell(i,j,k) = \begin{cases} 1 - q_{i,k}(1 - \Psi_{i,j,k}^{m_{i,j}}), & \ell = 0 \\ \frac{q_{i,k}\Gamma(\ell + m_{i,j})}{\ell! \Gamma(m_{i,j})} \left(\frac{\Omega_{i,j} C_{i,j,k}}{m_{i,j}}\right)^{\ell} \Psi_{i,j,k}^{m_{i,j}+\ell} & \ell > 0 \end{cases} \tag{26}$$

and

$$\Psi_{i,j,k} = \left(\beta_0 \frac{\Omega_{i,j} C_{i,j,k}}{m_{i,j}} + 1\right)^{-1}, \quad i \in \mathcal{S}_k, \quad 1 \le k \le 4. \tag{27}$$

IV. Numerical Results

In the following examples, performance metrics are calculated by using a Monte Carlo approach with N simulation trials. In each simulation trial, a realization of the network of Fig. 1 is obtained by placing M mobiles within it according to a uniform clustering distribution with each mobile having an exclusion-zone radius set equal to $d_0 = 0.004$ km. Randomly generated shadowing factors are used to associate mobiles with cell sectors and in other computations. The code rate permitted by the threshold is given by

$$R = \log_2(1 + l_s\beta) \tag{28}$$

where $l_s = 0.794$ corresponds to a 1 dB loss relative to the Shannon bound for complex discrete-time AWGN channels. The density of mobiles in a network of area A_{net} is $\lambda = M/A_{\text{net}}$. The outage probability ϵ_i of the reference link for simulation trial i is computed by applying (24)−(27). The *throughput* of the reference uplink for simulation trial i is $R(1-\epsilon_i)$. The average outage probability over all the simulation trials is

$$\overline{\epsilon} = \frac{1}{N}\sum_{i=1}^{N}\epsilon_i. \tag{29}$$

The maximum rate of successful data transmissions per unit area is characterized by the *area spectral efficiency*, defined as

$$\mathcal{A} = \lambda R(1-\overline{\epsilon}) \tag{30}$$

where the units are bits per channel use per unit area.

To avoid edge effects, the performance is measured for mobile stations placed in the yellow shaded area of Fig. 1, which is a 20 km by 20 km square located in the middle of the network. To consider the effect of base-station densification, the base-station deployment and the density of mobiles $\lambda = 20/km^2$ are maintained while the size of the network is scaled (dimensions redefined). For a fixed number of base stations, each scaling reduces the associated number of mobiles and decreases the transmission distances accordingly. In considering the effects of intersector interference, only the strongest 30 signals were used, as the attenuation of further signals was severe enough to make their individual effects negligible.

The slot duration is $T = 0.5$ ms, $P_r/\mathcal{N} = 30$ dB, $L/L_j = L/L_l = 10$, and $\mu = 40/km$. Each base station has $b = 0.01$ and $\zeta = 24$. Each mobile beamwidth is $\Theta = 0.1\pi$ radians and sidelobe level is $a = 0.1$, and the common activity factor is $p_i = 1$. The propagation parameters are $(m_{\max}, m_{\min}, \alpha_{\min}, \alpha_{\max}, \sigma_{\min}, \sigma_{\max}) = (2, 1, 2.3, 4.7, 6.1 \text{ dB}, 12.6 \text{ dB})$, which are suitable for an urban network. The reference signal has fading parameter $m_0 = 1$ when $d_r = 0.1$ km, and $m_0 = 2$ when $d_r = 0.01$ km. The ratio C/M serves as a measure of the densification of the base stations.

To capture the impact of densification, we need to take into account the decrease in the *typical link-length* d_r of the reference link and the consequent increase in Γ_0 as C/M increases. For a fixed density of mobiles, the average cell radius and hence a *typical* d_r are proportional to $1/\sqrt{C/M}$. For the range of C/M of interest, we consider

$$d_r = \frac{d_{r0}}{10\sqrt{C/M}}, \quad 0.01 \le C/M \le 1 \tag{31}$$

where d_{r0} is the typical link length when $C/M = 0.01$.

Fig. 3 depicts the average outage probability $\overline{\epsilon}$ for a typical link as a function of the densification for $d_{r0} = 0.1$ km, $\beta = 3$ dB, $N = 10^5$, distance-dependent fading, both shadowing and no shadowing ($\sigma_{\min} = \sigma_{\max} = 0$), and both frequency hopping and its absence. In the absence of frequency hopping, the reference signal is assumed to experience constant fading over a subframe, which is valid if subframe duration is less than the coherence time. The figure illustrates the reduced

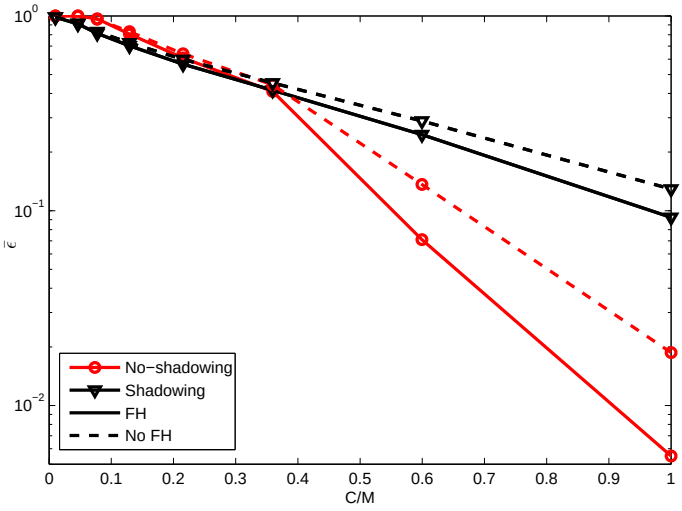

Fig. 3. Average outage probability for $d_{r0} = 0.1$ km, $\beta = 3$ dB, $N = 10^5$, and distance-dependent fading.

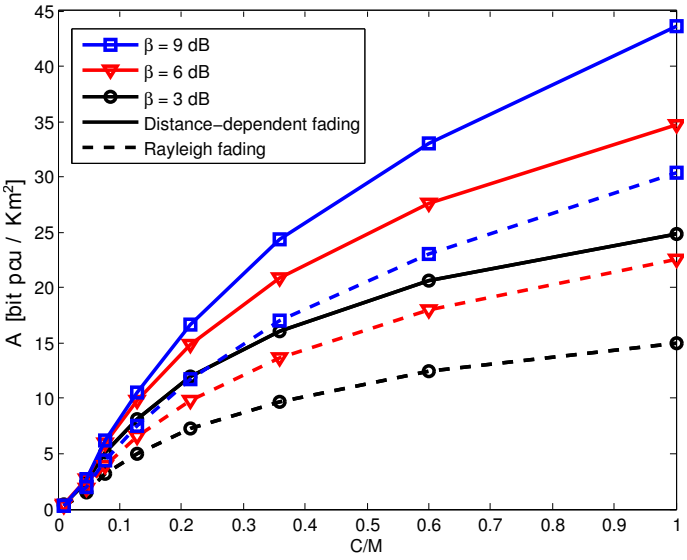

Fig. 4. Area spectral efficiency for three values of the SINR threshold, $d_{r0} = 0.1$ km, and $N = 10^5$.

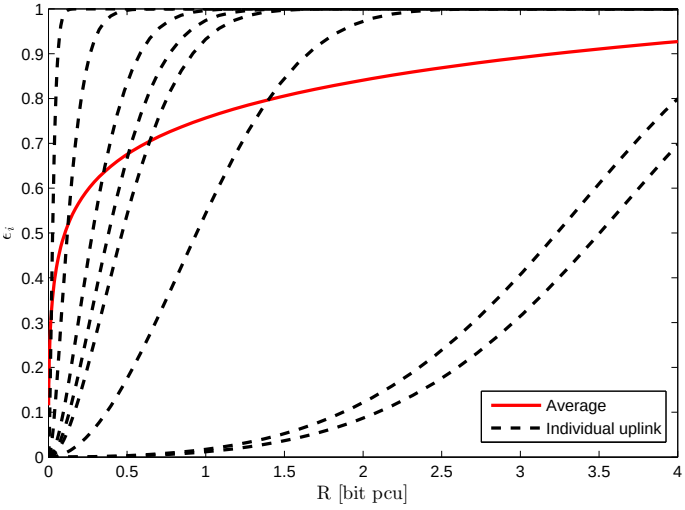

Fig. 5. Outage probability for eight uplinks and the average outage probability over all the uplinks for $C/M = 0.1$, $\beta = 3$ dB, distance-dependent fading, and a single simulation trial.

importance of frequency hopping in the presence of substantial shadowing because of the decrease in the typical values of Γ_0. The primary reasons for the monotonic decrease in $\overline{\epsilon}$ with densification and the increased importance of the frequency hopping are the increases in Γ_0 and the reduced shadowing and fading experienced by the reference signal. Calculations show that decreasing L/L_j has a very small detrimental effect, which indicates the minor importance of the intercell interference due to the sectorization and the narrow adaptive beams.

Fig. 4 depicts the area spectral efficiency $\mathcal{A}$ as a function of the densification for three values of the SINR threshold, $d_{r0} = 0.1$ km, and $N = 10^5$. Results are shown for both the distance-dependent fading and the more severe Rayleigh fading for which $m_{i,j} = m(d) = m_0 = 1$. Increases in the SINR threshold β of the network links increase the outage probability. However, for sufficiently large values of C/M and hence Γ_0, this effect is minor compared with increased code rate that can be accommodated. As a result, the area spectral efficiency increases significantly.

Fig. 5 shows the outage probability as a function of code-rate R for $C/M = 0.1$, $\beta = 3$ dB, distance-dependent fading, and a single simulation trial. The dashed lines in the figure were generated by selecting eight random uplinks in the network and computing each outage probability. The average over all the uplinks is represented by the solid line. Despite the use of power control, there is considerable variability in the dependence of the outage probability on the code rate due to the irregular network topology.

V. Conclusions

This paper derives an analytical model for calculating the outage probability and area spectral efficiency. The model includes the effects of millimeter-wave propagation, directional beams, frequency hopping, an arbitrary network topology, and the assignment of frequency blocks to mobiles. Numerical examples illustrate the effects of various features and parameters. Base-station densification improves the network performance significantly. The significance of the intercell interference is greatly reduced because of the highly directional sectorization and beamforming. The frequency hopping more effectively compensates for frequency-selective fading as the shadowing decreases. The area spectral efficiency increases with the code rate despite the increase in the outage probability.

References

[1] J. G. Andrews, S. Buzzi, C. Wan, S. V. Hanly, A. Lozano, A. C. K. Soong, and J. C. Zhang, "What will 5G be?," *IEEE J. Select. Areas Commun.*, vol. 32, pp. 1065–1082, June 2014.

[2] P. Wang, L. Yonghui, S. Lingyang, and B. Vucetic, "Multi-gigabit millimeter wave wireless communications for 5G: From fixed access to cellular networks," *IEEE Commun. Magazine*, vol. 53, pp. 168–178, January 2015.

[3] S. Deb and P. Monogioudis, "Learning-based uplink interference management in 4G LTE cellular systems," *IEEE/ACM Trans. Networking*, vol. 23, pp. 398–411, April 2015.

[4] N. Abu-Ali, "Uplink scheduling in LTE and LTE-Advanced: Tutorial, survey and evaluation framework," *IEEE Commun. Surveys and Tutorials*, vol. 16, pp. 1239–1265, third quarter 2014.

[5] G. Ku and J. M. Walsh, "Resource allocation and link adaptation in LTE and LTE advanced: A tutorial," *IEEE Commun. Surveys and Tutorials*, vol. 17, pp. 1605–1633, third quarter 2015.

[6] D. Torrieri and M. C. Valenti, "The outage probability of a finite ad hoc network in Nakagami fading," *IEEE Trans. Commun.*, vol. 60, pp. 3509–3518, November 2012.

[7] K. Zheng, L. Zhao, J. Mei, B. Shao, W. Xiang, and L. Hanzo, "Survey of large-scale MIMO systems," *IEEE Commun. Surveys and Tutorials*, vol. 17, pp. 1738–1760, third quarter 2015.

[8] S. Rangan, T. S. Rappaport, and E. Erkip, "Millimeter-wave cellular wireless networks: Potentials and challenges," *Proc. IEEE*, vol. 102, pp. 366–385, March 2014.

[9] M. R. Akdeniz, L. Yuanpeng, M. K. Samimi, S. Shu, S. Rangan, T. S. Rappaport, and E. Erkip, "Millimeter wave channel modeling and cellular capacity evaluation," *IEEE J. Select. Areas Commun.*, vol. 32, pp. 1164–1179, June 2014.

[10] T. S. Rappaport, G. R. MacCartney, M. K. Samimi, and S. Sun, "Wideband millimeter-wave propagation measurements and channel models for future wireless communication system design," *IEEE Trans. Commun.*, vol. 63, 2015.

[11] D. Torrieri, *Principles of Spread-Spectrum Communication Systems, 3rd ed.* New York: Springer, 2015.